Annals of Nuclear Medicine Vol. 20, No. 2, 139–146, 2006

Database of normal human cerebral blood flow measured by SPECT: II. Quantification of I-123-IMP studies with ARG method and effects of partial volume correction

Kentaro INOUE,* Hiroshi ITO,* Miho SHIDAHARA,* Ryoi GOTO,* Shigeo KINOMURA,* Kazunori SATO,* Yasuyuki TAKI,* Ken OKADA,* Tomohiro KANETA** and Hiroshi FUKUDA*

*Department of Nuclear Medicine and Radiology, Institute of Development, Aging and Cancer, Tohoku University
**Department of Radiology, Graduate School of Medicine, Tohoku University

The limited spatial resolution of SPECT causes a partial volume effect (PVE) and can lead to the significant underestimation of regional tracer concentration in the small structures surrounded by a low tracer concentration, such as the cortical gray matter of an atrophied brain. The aim of the present study was to determine, using ^{123}I-IMP and SPECT, normal CBF of elderly subjects with and without PVE correction (PVC), and to determine regional differences in the effect of PVC and their association with the regional tissue fraction of the brain. ***Methods:*** Quantitative CBF SPECT using ^{123}I-IMP was performed in 33 healthy elderly subjects (18 males, 15 females, 54–74 years old) using the autoradiographic method. We corrected CBF for PVE using segmented MR images, and analyzed quantitative CBF and regional differences in the effect of PVC using tissue fractions of gray matter (GM) and white matter (WM) in regions of interest (ROIs) placed on the cortical and subcortical GM regions and deep WM regions. ***Results:*** The mean CBF in GM-ROIs were 31.7 ± 6.6 and 41.0 ± 8.1 m*l*/100 g/min for males and females, and in WM-ROIs, 18.2 ± 0.7 and 22.9 ± 0.8 m*l*/100 g/min for males and females, respectively. The mean CBF in GM-ROIs after PVC were 50.9 ± 12.8 and 65.8 ± 16.1 m*l*/100 g/min for males and females, respectively. There were statistically significant differences in the effect of PVC among ROIs, but not between genders. The effect of PVC was small in the cerebellum and parahippocampal gyrus, and it was large in the superior frontal gyrus, superior parietal lobule and precentral gyrus. ***Conclusion:*** Quantitative CBF in GM recovered significantly, but did not reach values as high as those obtained by invasive methods or in the $H_2{}^{15}O$ PET study that used PVC. There were significant regional differences in the effect of PVC, which were considered to result from regional differences in GM tissue fraction, which is more reduced in the frontoparietal regions in the atrophied brain of the elderly.

Key words: ^{123}I-IMP, quantitative SPECT, cerebral blood flow, partial volume effect, tissue fraction

INTRODUCTION

QUANTITATION of regional cerebral blood flow (CBF) has been performed using single photon emission computed tomography (SPECT). However, because the limited spatial resolution of SPECT causes a partial volume effect (PVE), tracer concentration in brain structures can be underestimated in regions with a high tracer concentration relative to surroundings, and overestimation in regions with low tracer concentration.[1] In the CBF SPECT study, the PVE causes a volume averaging effect among gray matter (GM), white matter (WM) and cerebrospinal fluid (CSF) in a region of the brain. Quantitative SPECT underestimates CBF significantly compared with invasive techniques and positron emission tomography (PET), and one of the major causes of this underestimation has

Received July 19, 2005, revision accepted November 29, 2005.

For reprint contact: Kentaro Inoue, M.D., Ph.D., Department of Nuclear Medicine and Radiology, Institute of Development, Aging and Cancer, Tohoku University, 4–1 Seiryomachi Aoba-ku, Sendai 980–8575, JAPAN.

E-mail: kenta@idac.tohoku.ac.jp

been considered the PVE. Recently, several investigators have applied methods of PVE correction (PVC) using high-resolution anatomic magnetic resonance imaging (MRI) to PET[2–5] and SPECT,[6] and demonstrated that apparent differences resulting from regional morphological differences of the brain could be corrected and functional or pathophysiological differences could be detected following PVC.

N-isopropyl-*p*-[^{123}I]iodoamphetamine (^{123}I-IMP) has been widely used as a CBF tracer for SPECT. A method of quantitating CBF using ^{123}I-IMP and SPECT, the autoradiographic (ARG) method, has been developed as a method employing a two-compartment model, in which distribution volume (Vd) is assumed to be uniform in the brain and an arterial input function is obtained by the calibration of a standard input function by one-point arterial blood sampling.[7] Several studies have validated that the ARG method provides regional CBF significantly correlated to those obtained by $H_2{}^{15}O$ and positron emission tomography (PET), ^{133}Xe-SPECT and ^{123}I-IMP microsphere methods,[7,8] although these studies have also demonstrated the systematic underestimation of regional CBF in the cortical GM regions that is considered to be due to the PVE.

In the present study, we aim to determine normal CBF using ^{123}I-IMP and the ARG method in elderly subjects with and without PVC using MRI. We also aim to determine association of regional CBF with the regional tissue fraction of the brain.

MATERIALS AND METHODS

Subjects

Thirty-three healthy volunteers (18 males, mean age 65.3 ± 6.9 yr, range 55–74 yr; 15 females, mean age 64.3 ± 6.2 yr, range 54–71 yr) participated. They were participants in a research program on brain aging in city dwellers conducted by the Institute of Development, Aging and Cancer, Tohoku University. Only those with normal T1- and T2-weighted MR brain images, or minor hyperintensities on a T2-weighted image in the deep WM or periventricular WM, were recruited for this study. The study was approved by the local ethics committee of the Department of Medicine, Tohoku University. Written informed consent was obtained from all the subjects after a proper explanation of the study being conducted, according to the Code of Ethics of the World Medical Association (Declaration of Helsinki).

SPECT

SPECT scan was acquired at 30 min of mid-scan-time after the injection of 111 MBq ^{123}I-IMP. Image acquisition was performed with a three-head gamma camera (Multispect3, Siemens Medical Systems, Inc., Germany) equipped with a fan beam collimator. For each camera, projection data were acquired in a 128 × 128 format for 30 projections at 50 s with a 120° rotation of the camera. Image reconstruction was performed by filtered back-projection using a Butterworth filter (order, 8; cut-off frequency, 0.3 cycles/pixel) resulting in a spatial resolution of 10.6 mm. Attenuation correction was performed numerically, assuming an elliptical object for each slice and a uniform attenuation coefficient (0.08 cm^{-1}) (Chang's method). No correction was performed for scattered photons. Each subject was in the supine position during the injection and subsequent SPECT measurement. One-point arterial blood sampling from the brachial artery was performed 10 min after the injection. The radioactivity of the whole blood was measured with a well counter and used for calibration against the standard input function to obtain an arterial input function for the ARG method[7] to calculate a quantitative CBF SPECT image (ARG-CBF image). A cross-calibration scan was acquired using a cylindrical uniform phantom (20 cm in diameter and length) for the calibration of the relative sensitivities of the SPECT scanner and well counter system.

MR

All MR imaging studies were performed using a Signa 0.5-Tesla system (General Electric, Milwaukee, WI, USA). A three-dimensional volumetric acquisition of a T1-weighted gradient echo sequence produced a gapless series of thin transverse sections using an SPGR sequence (TE/TR, 7/40 ms; flip angle, 30°; 25-cm field of view; acquisition matrix, 256 × 256; slice thickness, 1.5 mm).

Data Processing and Analysis

We used Matlab 6.5.1 (Mathworks, Natick, MA, USA) and SPM2 (Wellcome Department of Cognitive Neurology, Institute of Neurology, London, UK: http://www.fil.ion.ucl.ac.uk/spm) for MR and SPECT image processing and statistical analysis. As described below in detail, a CBF SPECT image representing CBF for GM (GM-CBF image) was generated by subtracting CBF corresponding to that of WM from the ARG-CBF image. A CBF SPECT image with PVC (PVC-CBF image) was generated by dividing the GM-CBF image by a segmented and convolved MR image of GM. These processes are based on a method using a three compartment model developed for PVC for PET,[5] summarized in the following equation: $I_{GM} = (I_{OBS} - I_{WM}X_{WM}\otimes h - I_{CSF}X_{CSF}\otimes h)/X_{GM}\otimes h$, where I_{OBS} is the observed values for each voxel, I_{GM} , I_{WM} and I_{CSF} are SPECT images of the GM, WM and CSF, respectively, X_{GM}, X_{WM} and X_{CSF} are the spatial distribution of GM, WM and CSF voxels, respectively, $\otimes$ is a convolution operator, and h is the three-dimensional point spread function of the system. In practice, each whole brain MR image was segmented into GM, WM and CSF MR images by a clustering algorithm, calculating a Bayesian probability of belonging to each tissue for each voxel using a priori probability images of GM, WM and CSF with inhomogeneity correction for the

Fig. 1

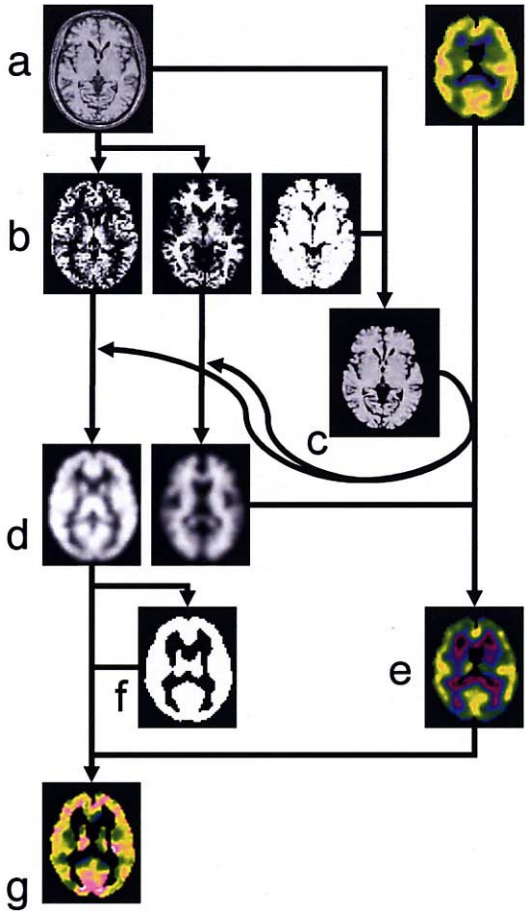

Fig. 1 Image processing procedures. a. original MR (*left*) and ARG-CBF (*right*) image, b. segmented images of gray (*left*) and white (*middle*) matter, and brain mask image to apply the original MR image, c. whole brain MR image was used for parameter estimation for co-registration of MR images to SPECT image. d. segmented MR images that were coregistered to SPECT image and smoothed; GM-MR image (*left*), WM-MR image (*right*), e. GM-CBF image created by subtraction of WM-CBF values using ARG-CBF and WM-MR images, f. GM-mask image, g. PVC-CBF image created by dividing GM-CBF image with GM-MR image, and applied GM-mask image.

Fig. 2 Seventeen spherical ROIs superimposed on the mean ARG-CBF image, which are shown as circles in their maximum diameters. The coordinates of center for ROIs on the standard space are: a) cerebellum (±27, −72, −30), b) parahippocampal gyrus (PHG) (±27, −9, −21), c) inferior temporal gyrus (ITG) (±57, −33, −21), d) thalamus (±12, −21, 3), e) lentiform (±27, 3, 3), f) superior temporal gyrus (STG) (±57, −27, 3), g) middle temporal gyrus (MTG) (±51, −63, 3), h) middle frontal gyrus (MFG) (±36, 51, 3), i) inferior frontal gyrus (IFG) (±42, 30, 3), j) cuneus (±15, −66, 3), k) anterior cingulate gyrus (AntCing) (±9, 30, 27), l) posterior cingulate gyrus (PostCing) (±9, −57, 27), m) superior frontal gyrus (SFG) (±15, 54, 27), n) inferior parietal lobule (IPL) (±57, −42, 27), o) precentral gyrus (PCG) (±36, −9, 54), p) superior parietal lobule (SPL) (±33, −54, 54), q) precuneus (±9, −51, 54).

Fig. 3 Mean image after spatial normalization of (a) ARG-CBF images, (b) PVC-CBF images, and (c) GM-MR images which were resliced and smoothed to approximate SPECT spatial resolution. Numbers in the bottom row indicate distance (in mm) from the AC-PC plane.

Fig. 2

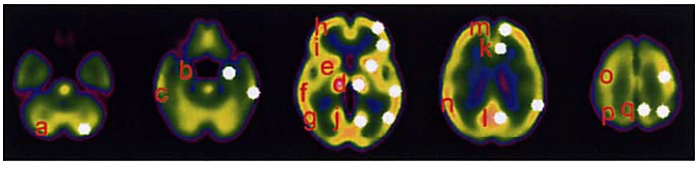

Fig. 3

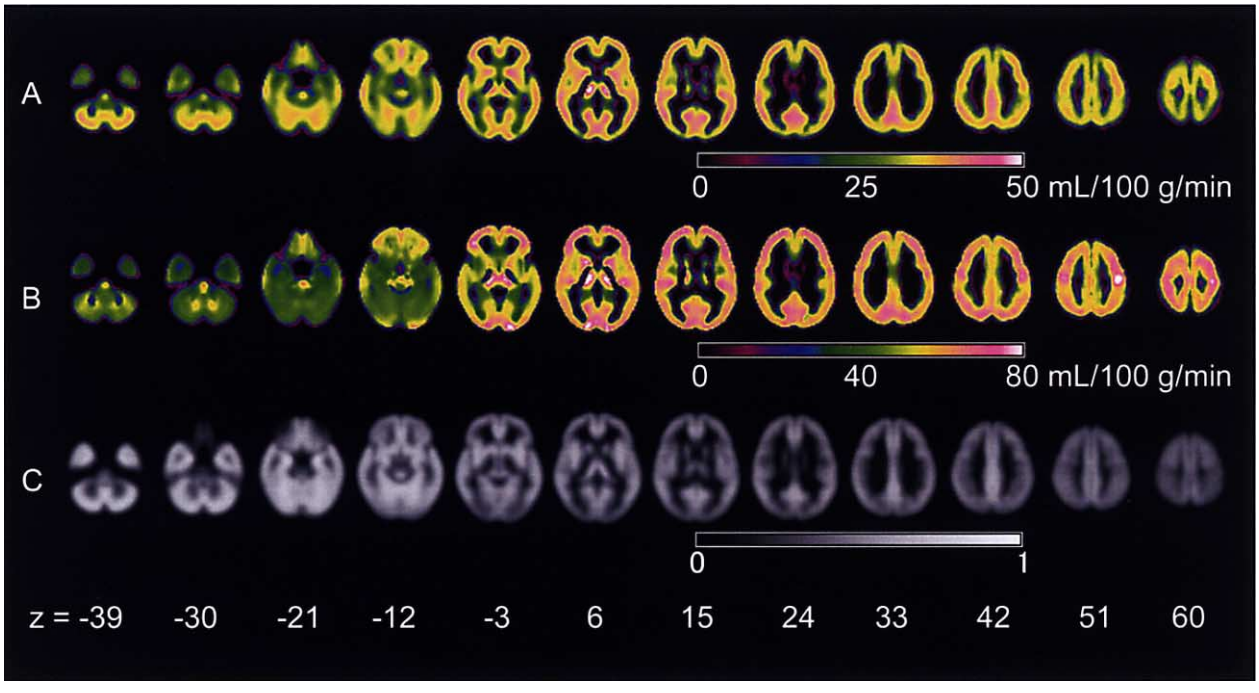

Table 1 Quantitative cerebral blood flow (CBF) using the autoradiographic (ARG) method for ^{123}I-IMP before (ARG-CBF) and after (PVC-CBF) partial volume correction (PVC)

ROI	ARG-CBF						PVC-CBF					
	Male		Female		Total		Male		Female		Total	
	Mean	SD	Mean	SD	Mean	SD	Mean	SD	Mean	SD	Mean	SD
SFG	29.6	4.9	37.9	6.9	33.4	7.2	57.8	10.7	72.1	15.3	64.3	14.7
MFG	33.5	6.4	41.9	6.9	37.4	7.8	60.5	10.9	75.0	12.7	67.1	13.8
IFG	33.3	5.8	41.7	6.6	37.1	7.4	59.0	10.6	74.1	11.4	65.9	13.3
PCG	32.2	5.1	40.9	7.4	36.2	7.6	59.6	10.5	76.2	15.0	67.2	15.1
precuneus	28.6	5.5	37.8	6.2	32.8	7.4	48.2	8.3	63.6	9.9	55.2	11.8
SPL	28.8	5.9	37.9	7.0	32.9	7.8	55.8	9.6	70.5	12.2	62.5	13.0
cuneus	34.6	5.5	44.9	7.0	39.3	8.0	54.1	9.1	74.3	15.8	63.2	16.1
IPL	32.6	6.3	42.7	8.0	37.2	8.7	54.8	9.0	68.3	9.8	60.9	11.5
STG	34.4	6.2	44.9	7.4	39.1	8.6	52.3	8.6	68.1	9.7	59.5	12.0
MTG	33.1	5.4	42.8	6.9	37.5	7.8	51.7	8.2	68.3	12.3	59.2	13.2
ITG	27.1	4.4	35.2	5.6	30.8	6.4	39.9	6.4	53.0	9.1	45.8	10.1
AntCing	25.3	4.3	34.5	5.6	29.5	6.7	36.6	6.4	49.9	9.0	42.7	10.1
PostCing	34.7	6.0	45.8	9.3	39.7	9.4	53.8	10.5	69.5	14.1	60.9	14.5
PHG	25.0	3.5	32.6	5.7	28.5	6.0	30.5	4.2	40.1	7.4	34.9	7.6
lentiform	35.7	5.9	45.1	7.5	40.0	8.1	48.4	7.5	61.3	11.3	54.3	11.4
thalamus	38.0	7.3	47.9	7.8	42.5	9.0	63.7	12.8	82.5	15.7	72.2	17.0
cerebellum	31.9	5.7	42.5	7.3	36.7	8.3	39.0	8.4	51.4	9.4	44.6	10.8
GM Total	31.7	6.6	41.0	8.1	35.9	8.7	50.9	12.8	65.8	16.1	57.7	16.2
WM	18.2	0.7	22.9	0.8	20.3	0.7	–	–	–	–	–	–

Abbreviations: see legends of Figure 2.

magnetic field (Fig. 1b).[9,10] These segmented images had values for each voxel ranging from 0 to 1, representing the tissue fraction of each tissue in each voxel. A binary brain mask for the whole brain obtained from the GM and WM images was applied to each whole brain MR image to remove the outer scalp to improve the coregistration of images (Fig. 1c). The whole and segmented MR images were co-registered to the SPECT image for each subject, and resliced to adjust to the voxel size of the SPECT image (2.9 × 2.9 × 2.9 mm) using the trilinear interpolation.[9] The resliced images were then convolved with a 9.6 mm FWHM isotropic Gaussian kernel, approximating the point spread function of the SPECT device to yield the GM-MR, WM-MR (Fig. 1d) and CSF-MR images.

The regions of interest (ROIs) of WM were automatically extracted from the WM-MR image as areas of more than 95% in WM concentration and then overlaid on the ARG-CBF image using MRIcro software[11] to acquire the mean CBF for the ROIs. A GM-CBF image (Fig. 1e) was obtained by subtracting the WM-CBF values that were calculated by the multiplication of the WM-MR image by the mean CBF for the WM-ROI, assuming that CBF is homogeneous throughout the WM, from the ARG-CBF image with use of the brain mask image for SPECT under the assumption that tracer retention in the CSF space is negligible.

To obtain a CBF image with the PVC (PVC-CBF image), the GM-CBF image was divided by the GM-MR image. A GM mask image (Fig. 1f) that consisted of voxels at which the GM concentration was larger than the empirically determined value of 0.25 in the GM-MR image was, then, applied to remove activities outside the brain and around the edge of GM, yielding the PVC-CBF

Table 2 Correction factors* for each region of interest (ROI)

ROI	Male		Female		Total	
	Mean	SD	Mean	SD	Mean	SD
SFG	2.0	0.2	1.9	0.1	1.9	0.2
MFG	1.8	0.1	1.8	0.1	1.8	0.1
IFG	1.8	0.1	1.8	0.1	1.8	0.1
PCG	1.9	0.2	1.9	0.1	1.9	0.1
precuneus	1.7	0.2	1.7	0.1	1.7	0.1
SPL	2.0	0.2	1.9	0.2	1.9	0.2
cuneus	1.6	0.1	1.6	0.1	1.6	0.1
IPL	1.7	0.1	1.6	0.1	1.7	0.1
STG	1.5	0.1	1.5	0.1	1.5	0.1
MTG	1.6	0.1	1.6	0.1	1.6	0.1
ITG	1.5	0.1	1.5	0.1	1.5	0.1
AntCing	1.5	0.2	1.4	0.1	1.4	0.1
PostCing	1.5	0.1	1.5	0.1	1.5	0.1
PHG	1.2	0.0	1.2	0.1	1.2	0.1
lentiform	1.4	0.1	1.4	0.1	1.4	0.1
thalamus	1.7	0.1	1.7	0.1	1.7	0.1
cerebellum	1.2	0.1	1.2	0.0	1.2	0.1
Total	1.6	0.3	1.6	0.2	1.6	0.2

* The correction factor was calculated as (PVC-CBF divided by ARG-CBF). Abbreviations: see legends of Figure 2.

Table 3 Regional tissue fraction for each region of interest (ROI)

ROI	Gray						White					
	Male		Female		Total		Male		Female		Total	
	Mean	SD	Mean	SD	Mean	SD	Mean	SD	Mean	SD	Mean	SD
SFG	0.35	0.05	0.38	0.04	0.37	0.04	0.48	0.06	0.45	0.06	0.46	0.06
MFG	0.43	0.05	0.44	0.05	0.43	0.05	0.41	0.06	0.41	0.06	0.41	0.06
IFG	0.42	0.04	0.42	0.03	0.42	0.04	0.46	0.05	0.46	0.05	0.46	0.05
PCG	0.38	0.06	0.38	0.05	0.38	0.06	0.48	0.07	0.48	0.07	0.48	0.07
precuneus	0.44	0.06	0.45	0.05	0.45	0.06	0.38	0.06	0.38	0.04	0.38	0.05
SPL	0.40	0.05	0.43	0.06	0.41	0.06	0.37	0.06	0.34	0.07	0.35	0.06
cuneus	0.52	0.05	0.49	0.04	0.51	0.05	0.37	0.05	0.41	0.05	0.38	0.06
IPL	0.49	0.05	0.52	0.06	0.50	0.06	0.34	0.05	0.32	0.06	0.33	0.06
STG	0.55	0.06	0.55	0.05	0.55	0.05	0.33	0.04	0.33	0.06	0.33	0.05
MTG	0.53	0.05	0.52	0.06	0.52	0.05	0.35	0.07	0.37	0.06	0.36	0.07
ITG	0.59	0.05	0.58	0.04	0.59	0.05	0.22	0.05	0.23	0.05	0.22	0.05
AntCing	0.41	0.05	0.43	0.04	0.42	0.05	0.42	0.05	0.42	0.04	0.42	0.04
PostCing	0.52	0.04	0.52	0.04	0.52	0.04	0.37	0.05	0.37	0.05	0.37	0.05
PHG	0.73	0.03	0.72	0.03	0.73	0.03	0.16	0.03	0.17	0.02	0.17	0.03
lentiform	0.62	0.06	0.61	0.05	0.62	0.05	0.34	0.06	0.36	0.05	0.35	0.06
thalamus	0.47	0.07	0.47	0.04	0.47	0.06	0.42	0.06	0.43	0.05	0.42	0.06
cerebellum	0.72	0.05	0.74	0.04	0.73	0.05	0.23	0.06	0.21	0.05	0.22	0.06
Total	0.50	0.12	0.51	0.11	0.51	0.12	0.36	0.10	0.36	0.10	0.36	0.10

Abbreviations: see legends of Figure 2.

image (Fig. 1g).

The ARG-CBF and PVC-CBF images and GM-MR and WM-MR images were spatially normalized to the ICBM 152 template (Montreal Neurological Institute), using linear and nonlinear parameters generated from spatial normalization of the original whole brain MR images.[12,13] These images were resliced at a final voxel size of 3 × 3 × 3 mm.

The comparison of SPECT images before and after the PVC, GM and WM-MR images was performed using the spatially normalized images. Seventeen spherical ROIs with 8 mm in diameter for GM (GM-ROI) were placed on the regions considered to be the GM regions of CBF SPECT images in each hemisphere referring to the mean ARG-CBF image (Fig. 2), and averaged for homologous ROIs in both hemispheres. To assign anatomical structures for GM-ROIs, WFU-PickAtlas software[14] was used. There should be GM, WM and CSF components with different fraction among these ROIs, which would relate to effect of the PVC. For each GM-ROI, therefore, mean CBF before and after the PVC and GM and WM concentrations were measured by averaging total voxel values in the whole ROI. To compare the regional effects of PVC, correction factors (CF) were calculated for each ROI as (PVC-CBF divided by ARG-CBF).

RESULTS

Quantitative CBF before and after PVC are summarized in Table 1. The mean ARG-CBF image is shown in Figure 3a. The mean CBF measured by the ^{123}I-IMP ARG method for all GM-ROIs were 31.7 ± 6.6 m*l*/100 g/min for males and 41.0 ± 8.1 m*l*/100 g/min for females, and for WM-ROI, 18.2 ± 0.7 m*l*/100 g/min for males and 22.9 ± 0.8 m*l*/100 g/min for females.

The mean PVC-CBF image is shown in Figure 3b, which illustrates that the PVC-CBF is higher in the upper part of the cortical GM but lower in the cerebellum and medial temporal lobe. The PVC-CBF for all GM-ROIs was 50.9 ± 12.8 m*l*/100 g/min for males and 65.8 ± 16.1 m*l*/100 g/min for females. Females showed significantly higher CBF than males ($p < 0.001$) in ARG-CBF and PVC-CBF.

There was a statistically significant difference in the CF (Table 2) among ROIs ($F(16,560) = 119.7$, $p < 0.001$), but not between genders ($F(1,560) = 0.435$, $p > 0.5$). The CFs were low in the cerebellum and parahippocampal gyrus compared with those in other ROIs except the lentiform nucleus, whereas they were high in the superior frontal gyrus (SFG), superior parietal lobule (SPL) and precentral gyrus (PCG) compared with those in other ROIs except the middle and inferior frontal gyri ($p < 0.001$, post hoc Sheffe's correction for multiple comparison).

Tissue fractions for all ROIs are summarized in Table 3. The mean GM fractions (Fig. 3c) for all GM-ROIs were 0.50 ± 0.12 for males and 0.51 ± 0.11 for females. The mean WM fractions for all GM-ROIs were 0.36 ± 0.10 for both males and females. Both showed a statistically significant main effect of ROI ($F(16,560) = 176.8$, $p < 0.001$ for GM, $F(16,560) = 96.9$, $p < 0.001$ for WM), but not a significant main effect of gender ($F(1,560) = 1.4$, $p > 0.2$ for GM, $F(1,560) = 0.1$, $p > 0.5$ for WM). The

GM fractions were highest in the cerebellum and parahippocampal gyrus and lowest in the SFG and PCG. The WM fractions showed an almost inverse relationship with GM fraction.

DISCUSSION

In this study, we performed PVC on the quantitative CBF SPECT images obtained using ^{123}I-IMP and the ARG method. We measured CBF before and after the PVC and found that CBF recovers significantly after PVC. We also demonstrated that there is a statistically significant difference in the effect of PVC between regions in the brain.

It has been widely accepted that the quantitative CBF averaged for the whole brain is approximately 50 m//100 g/min.[15] The measurements of the rate of clearance of ^{133}Xe from the brain after the injection of the radioisotope into the internal carotid artery suggested that there were two components in CBF. One was a fast component with a flow approximately 80 m//100 g/min and the other a slow component with a flow approximately 20 m//100 g/min,[16–18] which have been considered as CBF for GM and WM, respectively.

However the quantitative measurement of CBF using PET yields significantly underestimated CBF for the GM.[19–23] Iida et al. have shown that the primary cause of the underestimation of CBF in the cortical GM regions is PVE and the tissue heterogeneity within an ROI, and that if the GM and WM compartments are modeled for the calculation of CBF, CBF for GM will be comparable to those obtained by invasive techniques.[24]

Regarding SPECT, ^{123}I-IMP has a higher first pass extraction ratio than frequently used ^{99m}Tc-labeled CBF tracers and provides more precise estimates of the true CBF.[25] Quantitative CBF measured by ^{123}I-IMP and SPECT, however, have been reported as approximately 35 m//100 g/min for the cerebral cortex and 25 m//100 g/min for the centrum semiovale.[26] It has also been indicated that the CBF in the GM regions measured using ROIs were less than twice compared with those in the WM.[26] The total mean quantitative CBF of the GM-ROIs was 35.9 ± 8.7 m//100 g/min, and that of the WM-ROIs was 20.3 ± 0.7 m//100 g/min, which are consistent with those in the previous study.[26] The significantly higher CBF in women in this study was also consistent with several studies using different techniques.[26–28] The differences in CBF between genders were larger than those reported in those previous studies, although the causes of the larger gender differences in ARG-CBF values were not clear. The underestimation of CBF for the GM and the overestimation of CBF for the WM have been considered to be due to PVE of SPECT and the limited first pass extraction of ^{123}I-IMP.

In the present study, we found that GM concentrations in ROIs placed in regions in the mean ARG-CBF image, which were considered to represent CBF for GM, ranged from ~ 40% to as high as 60% in a large part of the cerebral cortex. Those ROIs also had a range of WM concentrations from about 30% to less than 50%. The values measured with ROI are biased by the size, shape, and location of the ROI, so if we had placed ROIs that differed in size or shape in different regions, the quantitative values could somewhat differ from the present results. In this study, we placed ROIs by referring to several previous studies that showed quantitative CBF using SPECT or PET,[19,20,26] and we considered that the ROIs we used here were common in clinical settings. The present result demonstrates that CBF in the GM regions of the SPECT images, generally, reflects only about 51% the GM fraction, 36% WM fraction, and the rest, CSF.

By adopting PVC, the corrected CBF increased by about 1.2–2.0 times that of the ARG-CBF, depending on the ROI, and the total mean PVC-CBF of GM-ROI became 57.7 ± 16.2 m//100 g/min. These values, nonetheless, were still underestimated compared with those obtained by invasive methods[16–18] and in $H_2{}^{15}O$ PET CBF studies that used PVC.[24,29] One of the reasons for this would be the low first pass extraction fraction of ^{123}I-IMP, particularly at high CBF,[30] which resulted in the CBF underestimation. The effects of scattered photons could be another reason for the CBF underestimation after PVC. It has been demonstrated that scatter correction improves CBF underestimation in the GM and CBF overestimation in the WM.[31] As described in the Methods section, we did not perform scatter correction, due to our instrumental limitations, and we subtracted WM-CBF from ARG-CBF. A WM-CBF was measured using ROIs consisting of voxels that had a WM tissue fraction >95% for each subject. This value would contain scatter components and be overestimated. The subtraction of these overestimated WM-CBF from the ARG-CBF results in the underestimation of GM-CBF, and therefore, in the underestimation of PVC-CBF.

Another reason for the underestimation of CBF would be nonlinearity in the parameter estimation apart from PVE, because the estimated parameter from the mixture of different tissues will not be equal to the simple average of the parameters constituting the mixture[32]; the nonlinear characteristics of the ARG method of ^{123}I-IMP have been shown to result in the CBF underestimation due to the gray-white mixture effect.[33] As we have reported previously, if GM tissue fraction of an ROI is 40–60%, like in the present study, and if the true CBF in GM is in the range of 60–100 m//100 m//min, the magnitude of underestimation of CBF by the ARG method, then, would be 10–25%.[34]

The corrected CBF were higher in the upper part of the cerebral cortex, and relatively low in the temporal cortex and cerebellum. This tendency in our results, but not the quantitative values, is consistent with that obtained in quantitative CBF studies using invasive techniques that reported lower CBF in regions that are considered to

correspond to the temporal lobe.[16,18] Few studies showed regional differences in the effect of PVC, which we assessed using CF in this study. Matsuda et al. illustrated in their fourth figure relative increases in regional CBF in the frontal and parietal cortices and decreases in the medial temporal lobe and cerebellum, in a comparison of before and after PVC in a CBF SPECT study.[6] Our present results were consistent with their results.[6] These findings could be due to the fact that GM atrophy has been noted predominantly in the frontal and parietal cortices,[35–37] but not observed,[37] or only mildly observed[36] in the medial temporal cortex in healthy elderly. As a limitation of this study, as we did not perform scatter correction, and thus the underestimation of CBF could have been relatively larger in the cortex than the deep gray matter, and also in structures in lower and higher slices than in the midlevel slices, due to the cross-sectional size of the scattering material.[31] The scatter correction, thus, could have affected regional difference in ARG-CBF and PVC-CBF. Meltzer et al., on the other hand, demonstrated that the effect of PVC in the medial temporal cortex and cerebellum are similar to those of other cortical regions as well as the thalamus and basal ganglia in their $H_2{}^{15}O$ PET CBF study using the two-compartment model.[29] The two-compartment model was less sensitive than the three-compartment model to errors in segmentation, white matter inhomogeneity, and image registration accuracy, but the effect of white matter inhomogeneity and image registration accuracy was relatively tolerated even with use of the three compartment model with poorer resolution data.[38] In the present study, we used the three-compartment model[5] due to its high recovery coefficient of GM radioactivity. The effect of PVC in the present study should be smaller in the medial temporal lobe and cerebellum than in other regions, differing from a study based on the two-compartment model,[29] because the diluting effect of WM should be smaller in these regions due to their smaller WM tissue fraction. Another limitation could be accuracy of segmentation of brain tissues. The segmentation procedure used in the present study was subjective and reproducible by using well-established software, SPM2. The existence of a certain number of mixed voxels due to PVE in the MRI images, however, remains an issue to be addressed. The exceptionally high GM fraction, and therefore low effect of PVC, in the medial temporal lobe and cerebellum could be due to, at least partly, segmentation inaccuracy caused by PVE in the MRI image. It is possible to improve MR segmentation between GM and WM in the cerebellum, which would require larger contrast in signal intensity between GM and WM as well as finer spatial resolution, by using MRI equipment with a higher magnetic field. The assessment of regional differences in MR segmentation quality is, however, a subject for further studies.

In conclusion, we applied PVC for quantitative CBF SPECT using ^{123}I-IMP in healthy elderly subjects. Our data demonstrated that quantitative CBF in GM recovers significantly, although it does not reach values as high as those obtained by invasive methods or in a $H_2{}^{15}O$ PET study that applied PVC. We also found that there is a significant regional difference in the effect of PVC among the cerebral cortical areas, which was considered to result from the regional difference in GM tissue fraction, which would be more reduced in the frontoparietal regions than in other regions in the atrophied brain of the elderly. Further studies are required to overcome several limitations in the present study, such as non-linear underestimation in CBF with use of ^{123}I-IMP-ARG method, effects of scatter photons, and inaccuracy of MR tissue segmentation.

ACKNOWLEDGMENTS

We are very thankful to the technical staff in Tohoku University Hospital for data acquisition. This work was partially supported by the Japanese Ministry of Education, Science, Sports and Culture, Grant-in-Aid for Young Scientists (B), 14770439, a grant from the Telecommunications Advancement Organization of Japan, a grant from the Future Medical Engineering based on Bio-nanotechnology (21th Century COE Program), Tohoku University, and a fund from Nihon Medi-Physics Co., Ltd.

REFERENCES

1. Hoffman EJ, Huang SC, Phelps ME. Quantitation in positron emission computed tomography: 1. Effect of object size. *J Comput Assist Tomogr* 1979; 3: 299–308.
2. Labbe C, Froment JC, Kennedy A, Ashburner J, Cinotti L. Positron emission tomography metabolic data corrected for cortical atrophy using magnetic resonance imaging. *Alzheimer Dis Assoc Disord* 1996; 10: 141–170.
3. Meltzer CC, Zubieta JK, Brandt J, Tune LE, Mayberg HS, Frost JJ. Regional hypometabolism in Alzheimer's disease as measured by positron emission tomography after correction for effects of partial volume averaging. *Neurology* 1996; 47: 454–461.
4. Ibanez V, Pietrini P, Alexander GE, Furey ML, Teichberg D, Rajapakse JC, et al. Regional glucose metabolic abnormalities are not the result of atrophy in Alzheimer's disease. *Neurology* 1998; 50: 1585–1593.
5. Muller-Gartner HW, Links JM, Prince JL, Bryan RN, McVeigh E, Leal JP, et al. Measurement of radiotracer concentration in brain gray matter using positron emission tomography: MRI-based correction for partial volume effects. *J Cereb Blood Flow Metab* 1992; 12: 571–583.
6. Matsuda H, Ohnishi T, Asada T, Li ZJ, Kanetaka H, Imabayashi E, et al. Correction for partial-volume effects on brain perfusion SPECT in healthy men. *J Nucl Med* 2003; 44: 1243–1252.
7. Iida H, Itoh H, Nakazawa M, Hatazawa J, Nishimura H, Onishi Y, et al. Quantitative mapping of regional cerebral blood flow using iodine-123-IMP and SPECT. *J Nucl Med* 1994; 35: 2019–2030.
8. Iida H, Akutsu T, Endo K, Fukuda H, Inoue T, Ito H, et al. A multicenter validation of regional cerebral blood flow

quantitation using [^{123}I]iodoamphetamine and single photon emission computed tomography. *J Cereb Blood Flow Metab* 1996; 16: 781–793.
9. Ashburner J, Friston K. Multimodal image coregistration and partitioning—a unified framework. *Neuroimage* 1997; 6: 209–217.
10. Ashburner J, Friston KJ. Voxel-based morphometry—the methods. *Neuroimage* 2000; 11: 805–821.
11. Rorden C, Brett M. Stereotaxic display of brain lesions. *Behav Neurol* 2000; 12: 191–200.
12. Ashburner J, Neelin P, Collins DL, Evans A, Friston KJ. Incorporating prior knowledge into image registration. *Neuroimage* 1997; 6: 344–352.
13. Ashburner J, Friston KJ. Nonlinear spatial normalization using basis functions. *Hum Brain Mapp* 1999; 7: 254–266.
14. Maldjian JA, Laurienti PJ, Kraft RA, Burdette JH. An automated method for neuroanatomic and cytoarchitectonic atlas-based interrogation of fMRI data sets. *Neuroimage* 2003; 19: 1233–1239.
15. Lassen NA. Normal average value of cerebral blood flow in younger adults is 50 ml/100 g/min. *J Cereb Blood Flow Metab* 1985; 5: 347–349.
16. Ingvar DH, Cronqvist S, Ekberg R, Risberg J, Hoedt-Rasmussen K. Normal values of regional cerebral blood flow in man, including flow and weight estimates of gray and white matter. A preliminary summary. *Acta Neurol Scand Suppl* 1965; 14: 72–78.
17. Hoedt-Rasmussen K. Regional cerebral flow in man measured externally following intra-arterial administration of 85-Kr or 133-Xe dissolved in saline. *Acta Neurol Scand Suppl* 1965; 14: 65–68.
18. Wilkinson IM, Bull JW, Duboulay GH, Marshall J, Russell RW, Symon L. Regional blood flow in the normal cerebral hemisphere. *J Neurol Neurosurg Psychiatry* 1969; 32: 367–378.
19. Hatazawa J, Fujita H, Kanno I, Satoh T, Iida H, Miura S, et al. Regional cerebral blood flow, blood volume, oxygen extraction fraction, and oxygen utilization rate in normal volunteers measured by the autoradiographic technique and the single breath inhalation method. *Ann Nucl Med* 1995; 9: 15–21.
20. Pantano P, Baron JC, Lebrun-Grandie P, Duquesnoy N, Bousser MG, Comar D. Regional cerebral blood flow and oxygen consumption in human aging. *Stroke* 1984; 15: 635–641.
21. Yamaguchi T, Kanno I, Uemura K, Shishido F, Inugami A, Ogawa T, et al. Reduction in regional cerebral metabolic rate of oxygen during human aging. *Stroke* 1986; 17: 1220–1228.
22. Leenders KL, Perani D, Lammertsma AA, Heather JD, Buckingham P, Healy MJ, et al. Cerebral blood flow, blood volume and oxygen utilization. Normal values and effect of age. *Brain* 1990; 113 (Pt 1): 27–47.
23. Kanno I, Iida H, Miura S, Murakami M, Takahashi K, Sasaki H, et al. A system for cerebral blood flow measurement using an $H_2{}^{15}O$ autoradiographic method and positron emission tomography. *J Cereb Blood Flow Metab* 1987; 7: 143–153.
24. Iida H, Law I, Pakkenberg B, Krarup-Hansen A, Eberl S, Holm S, et al. Quantitation of regional cerebral blood flow corrected for partial volume effect using O-15 water and PET: I. Theory, error analysis, and stereologic comparison. *J Cereb Blood Flow Metab* 2000; 20: 1237–1251.
25. Di Rocco RJ, Silva DA, Kuczynski BL, Narra RK, Ramalingam K, Jurisson S, et al. The single-pass cerebral extraction and capillary permeability-surface area product of several putative cerebral blood flow imaging agents. *J Nucl Med* 1993; 34: 641–648.
26. Hatazawa J, Iida H, Shimosegawa E, Sato T, Murakami M, Miura Y. Regional cerebral blood flow measurement with iodine-123-IMP autoradiography: normal values, reproducibility and sensitivity to hypoperfusion. *J Nucl Med* 1997; 38: 1102–1108.
27. Gur RC, Gur RE, Obrist WD, Hungerbuhler JP, Younkin D, Rosen AD, et al. Sex and handedness differences in cerebral blood flow during rest and cognitive activity. *Science* 1982; 217: 659–661.
28. Rodriguez G, Warkentin S, Risberg J, Rosadini G. Sex differences in regional cerebral blood flow. *J Cereb Blood Flow Metab* 1988; 8: 783–789.
29. Meltzer CC, Cantwell MN, Greer PJ, Ben-Eliezer D, Smith G, Frank G, et al. Does cerebral blood flow decline in healthy aging? A PET study with partial-volume correction. *J Nucl Med* 2000; 41: 1842–1848.
30. Kuhl DE, Barrio JR, Huang SC, Selin C, Ackermann RF, Lear JL, et al. Quantifying local cerebral blood flow by *N*-isopropyl-*p*-[^{123}I]iodoamphetamine (IMP) tomography. *J Nucl Med* 1982; 23: 196–203.
31. Iida H, Narita Y, Kado H, Kashikura A, Sugawara S, Shoji Y, et al. Effects of scatter and attenuation correction on quantitative assessment of regional cerebral blood flow with SPECT. *J Nucl Med* 1998; 39: 181–189.
32. Huang SC, Mahoney DK, Phelps ME. Quantitation in positron emission tomography: 8. Effects of nonlinear parameter estimation on functional images. *J Comput Assist Tomogr* 1987; 11: 314–325.
33. Ito H, Ishii K, Atsumi H, Inukai Y, Abe S, Sato M, et al. Error analysis of autoradiography method for measurement of cerebral blood flow by ^{123}I-IMP brain SPECT: a comparison study with table look-up method and microsphere model method. *Ann Nucl Med* 1995; 9: 185–190.
34. Ito H, Shidahara M, Inoue K, Goto R, Kinomura S, Taki Y, et al. Effects of tissue heterogeneity on cerebral vascular response to acetazolamide stress measured by an I-123-IMP autoradiographic method with single-photon emission computed tomography. *Ann Nucl Med* 2005; 19: 251–260.
35. Raz N, Gunning FM, Head D, Dupuis JH, McQuain J, Briggs SD, et al. Selective aging of the human cerebral cortex observed *in vivo*: differential vulnerability of the prefrontal gray matter. *Cereb Cortex* 1997; 7: 268–282.
36. Resnick SM, Pham DL, Kraut MA, Zonderman AB, Davatzikos C. Longitudinal magnetic resonance imaging studies of older adults: a shrinking brain. *J Neurosci* 2003; 23: 3295–3301.
37. Good CD, Johnsrude IS, Ashburner J, Henson RN, Friston KJ, Frackowiak RSJ. A voxel-based morphometric study of ageing in 465 normal adult human brains. *Neuroimage* 2001; 14: 21-36.
38. Meltzer CC, Kinahan PE, Greer PJ, Nichols TE, Comtat C, Cantwell MN, et al. Comparative evaluation of MR-based partial-volume correction schemes for PET. *J Nucl Med* 1999; 40: 2053–2065.